Journal of Photochemistry & Photobiology, A: Chemistry 435 (2023) 114294

Contents lists available at ScienceDirect

Journal of Photochemistry & Photobiology, A: Chemistry

journal homepage: www.elsevier.com/locate/jphotochem

The photocatalytic performance of Fe inserted in Nb_2O_5 obtained by microwave-assisted hydrothermal synthesis: Factorial design of experiments

Cátia Liane Ücker [a,*], Vitor Goetzke [a], Fábio Calcagno Riemke [a], Marcely Echeverria Oliveira [a], Neftali Lenin Villarreal Carreno [a], Fernando Dal Pont Morisso [b], Marcio Daldin Teodoro [c], Valmor R. Mastelaro [d], Mário Lúcio Moreira [a], Cristiane Wienke Raubach [a], Sergio da Silva Cava [a]

[a] Graduate Program in Materials Science and Engineering, Technological Development Center, Universidade Federal de Pelotas, 96010-610 Pelotas, RS, Brazil
[b] Postgraduate in Materials Technology and Industrial Processes, Universidade Feevale, 93525-075 Novo Hamburgo, RS, Brazil
[c] Department of Physics, Universidade Federal de São Carlos, 13565-905 São Carlos, SP, Brazil
[d] São Carlos Institute of Physics, Universidade de São Paulo, PO Box 369, 13560-970 São Carlos, SP, Brazil

ARTICLE INFO

Keywords:
Fe-insertion Nb_2O_5
Microwave-assisted hydrothermal
Rhodamine B
Photocatalysis
Factorial design of experiments

ABSTRACT

Nb_2O_5 and Fe inserted Nb_2O_5 from 1 to 3 % were synthesized by the microwave-assisted hydrothermal method. The XRD results confirm the presence of Nb_2O_5 with low crystallinity in all samples, which is characteristic of the material that was not subjected to heat treatment. The SEM images show that the insertion of Nb_2O_5 with Fe promotes the formation of pores on the surface of the material. The addition of Fe also led to a decrease in the band gap to pure Nb_2O_5. The photocatalytic performance for the degradation of rhodamine B was evaluated. The 1 %Fe-Nb_2O_5 sample showed the best photocatalytic discoloration result, achieving 100 % discoloration of RhB within 60 min. The increase in ion concentration leads to a decrease in photocatalytic performance. A 2^4 factorial design experiment was performed for samples of Nb_2O_5 and Nb_2O_5 with 1 %Fe-Nb_2O_5. The study variables were catalyst type (Nb_2O_5 and 1 %Fe-Nb_2O_5), catalyst dosage (25 and 50 mg), pH of the RhB solution (5 and 10), and time of photocatalytic analysis (30 and 60 min) to check the effect on the RhB discoloration. The analysis showed that the change in catalyst, catalyst dosage, pH and reaction time had a significant effect. Most of the interactions between the variables also had a significant effect on the process, both positively and negatively. The diversification of the results of the factorial design, variables, and their interactions allowed us to identify the best execution routes of heterogeneous photocatalysis for the removal of RhB, depending on the parameters used in this work.

1. Introduction

One of the major problems in the environment is water pollution, which is usually due to the disposal of industrial wastewater in inappropriate places, causing various consequences for the environment [1–3]. Industrial wastewater contains a large number of dyes used in various industries, such as paint, food, paper, textile, and others. [4,5]. Some methods aim to eliminate and/or reduce these types of consequences. One of these methods is heterogeneous photocatalysis, which is considered an advanced oxidative process (AOP) and aims to use catalytic materials, usually semiconductors, capable of degrading chemicals contained in wastewater upon irradiation [6–9]. For this purpose, the semiconductor material is excited, causing electrons to pass from the valence band (VB) to the conduction band (CB), forming pairs of electrons and holes that are used together with reactive species for photochemical degradation of organic compounds [10–12].

Various semiconductors have been used for this purpose and have been studied for several years. Modifications are often made to these materials to improve them and thus enable them to degrade organic compounds in a shorter time [13,14]. Niobium pentoxide (Nb_2O_5) is an *n*-type semiconductor [7,10] that has been reported in the literature to be a good catalyst for photocatalysis [7,8,15] as well as solar cells [16,17], sensors [18,19], catalysis [20,21], and other applications. The great feature of Nb_2O_5 is that it has very interesting chemical and

* Corresponding author.
E-mail address: catiaucker@gmail.com (C.L. Ücker).

https://doi.org/10.1016/j.jphotochem.2022.114294
Received 18 April 2022; Received in revised form 2 September 2022; Accepted 18 September 2022
Available online 23 September 2022

physical properties. It has a large band gap and is thermally stable and very corrosion resistant [7,22,23]. Nb_2O_5 is a material that can be obtained in a versatile way by various synthesis methods [24]. Microwave-assisted hydrothermal synthesis (MAH) enables the extraction of Nb_2O_5 at low temperatures in a relatively short time with uniform and volumetric heating [25,26]. This shows that this synthesis method proves to be advantageous over other methods, which usually require a long reaction time and higher temperatures [24]. The possibility of obtaining Nb_2O_5 at low temperatures makes it possible to find a material with low crystallinity, which favors a much more detailed study, mainly concerned with how the crystallinity of this material evolves as a function of the influence of the heat treatment temperature, which has already been studied in several works [25,27,28].

The photogenerated charges of Nb_2O_5 and TiO_2, which are also frequently used in these photocatalytic processes, have a very high tendency to recombine, which is unfavorable for photocatalysis [14]. One of the ways to improve the properties of materials is to introduce defects in the electronic structure of Nb_2O_5 [10]. Insertion with certain ions can improve the ability of materials to absorb light, which consequently favors charge transfer due to increased adsorption capacity on the surface of the catalyst material, leading to a better photocatalytic response [1,7,12]. Moreover, the incorporation of dopants or excess dopants may contribute to the formation of a recombination center, which affects the photocatalytic response. [14,29]. Various semiconductors modified with different ions can be found in the literature. However, the insertion of dopants in Nb_2O_5 and the effect in photocatalytic activity, mainly iron, is still scarce. Iron insertion could be an alternative to improve the photocatalytic activity of Nb_2O_5 by absorbing light at a higher wavelength [30,31].

In photocatalysis, numerous factors can affect the performance of a particular material. Experimental tests must be performed to identify and understand the parameters that may affect the photocatalytic response of a particular material [16]. The factorial design technique helps to identify the variables that most affect the photocatalysis process by determining the effect of each factor on the process response and the interaction of different factors. As a result, the number of experiments can be reduced, and thus better process optimization can be achieved [15,16,32–34].

Thus, in this work, Nb_2O_5 and Nb_2O_5 with different concentrations of Fe ions (1, 2, and 3 %) were synthesized by MAH synthesis and characterized in different analyses to verify the properties of these materials to be used later in heterogeneous photocatalysis tests against the dye rhodamine B. Moreover, a statistical method was performed with a 2^4 factorial design at two levels (−1 and +1), considering as process variables the use of Nb_2O_5 and 1 % iron inserted with Nb_2O_5, the amount of catalyst, the pH of the solution and finally the time of the process, resulting in a total of 16 experiments.

2. Materials and methods

2.1. Synthesis

The materials used in the synthesis were ammonium niobium oxalate ($NH_4[NbO(C_2O_4)_2(H_2O)]$. ($H_2O$)n supplied by Brazilian Company of Mining and Metallurgy, CBMM, Brazil), hydrogen peroxide (H_2O_2, 30 %, Synth), iron(III) nitrate nonahydrate ($FeN_3O_9{\cdot}9H_2O$, Sigma–Aldrich) and distilled water.

The synthesis method used to obtain pure Nb_2O_5 and Fe-Nb_2O_5 was the microwave-assisted hydrothermal method. For the Nb_2O_5 synthesis, 0.1 mol of ammonium niobium oxalate was dissolved in 30 mL of distilled water under constant stirring·H_2O_2 was added to the solution (molar ratio Nb:H_2O_2 was 1:10) while stirring for 10 min. The resulting solution was placed in a reactor coupled with a conventional microwave, and the synthesis was carried out at a constant temperature of 140 °C for 15 min. The pressure and temperature were monitored throughout the synthesis. The precipitate obtained was subjected to a washing and centrifugation process (repeated three times) to remove impurities and neutralize the pH. The material was oven-dried for 3 h at 100 °C.

For the Fe-Nb_2O_5, iron (III) nitrate nonahydrate was mixed into the solution to obtain 1, 2, and 3 % wt of Fe. Afterward, the entire synthesis procedure, as well as the operating conditions, were repeated as explained in the pure Nb_2O_5 synthesis.

2.2. Characterization

X-ray diffraction was performed using a Shimadzu 6000 XRD (XRD, Shimadzu, Japan) with CuKα radiation (1.5418 Å) at 30 kV and 30 mA, scanning from 2θ of 10°– 80°, with a 0.02° step and sweep speed of 2°/min. The chemical analysis by energy dispersive X-ray analysis (EDAX) was performed on a Shimadzu spectrometer model EDX-720. Micro-Raman spectroscopy analysis was performed in an iHR550 spectrometer (Horiba Jobin Yvon, Japan) coupled to a CCD detector and an Ag ion laser (MellesGriot, USA) with an excitation wavelength of 514.5 nm, a maximum power of 200 mW and a fiber microscope. Fourier transform infrared spectra (FTIR) were obtained in an IR-Prestige (Model 21, Shimadzu, Japan), and the sample was run at an infrared region between 4000 and 600 cm^{-1}. SEM analyses were performed with a JEOL JSM 6510 LV electron microscope operating at 10 kV. The specific surface areas of the powders were calculated by BET (Brunauer–Emmett–Teller) method from the adsorption isotherms in Nova2200e (Quantachrome). The transmission electron microscopy (TEM) analysis was performed in an electron microscope (JEM- 1400, JEOL, Japan) with an acceleration voltage of 120 kV.

The diffuse reflectance spectra were obtained by a UV–Vis spectrometer (HR2000 +, OCEAN OPTICS) in the wavelength range of 200–800 nm. The optical bandgap of the samples was estimated by the Tauc method for an indirect semiconductor $(\alpha h\nu)^{0.5}$ versus $h\nu$. Zeta potential analyses were prepared with a dispersion of 1 % catalyst in ultrapure water and were performed in a Nanobrook 90plus Pals device (Brookhaven). The photoluminescence (PL) measurements of the samples were excited by a 355 nm laser (Cobolt/Zouk) with the signal dispersed and detected by a 19.3 cm spectrometer and a Si-CCD detector (Andor Kymera/Idus), respectively.

The chemical surface analysis for the Nb_2O_5 and Fe-Nb_2O_5 samples was performed by X-ray photoelectron spectroscopy (XPS) using a conventional XPS spectrometer (ScientaOmicron ESCA +) with a high-performance hemispheric analyzer (EAC2000) with monochromatic Al Kα ($h\nu = 1486.6$ eV) radiation as the excitation source. The operating pressure in the ultra-high vacuum chamber (UHV) during the analysis was around 10^{-9} Pa. The XPS high-resolution spectra was recorded at a constant pass energy of 20 eV with 0.05 eV per step for the high-resolution spectra. A charge neutralizer (CN10) was used to exclude the surface charging effects. The obtained spectra were corrected assuming 284.8 eV for adventitious carbon and the analysis of the XPS spectra was realized by using CASA XPS software.

2.3. Photocatalytic activity

The photocatalytic activity of the samples was determined using a rhodamine B (RhB) dye solution ($1x10^{-5}$ M). For the tests, 50 mg of each sample was dissolved in 50 mL of RhB dye. The analysis was performed in a closed box illuminated by 5 UVC lamps (15 W each lamp totaling the power of 75 W - TUV Philips) with an intensity of 254 nm. First, all samples were stirred in the dark for 20 min to achieve equilibrium between the dye and the semiconductor material. After 20 min, the light was turned on, an aliquot was removed, referring to the starting point, and the other aliquots were withdrawn at 10-minute intervals until reaching a time of 60 min. All samples were centrifuged to separate the powder from the solution and then analysed in a UV–Vis spectrophotometer. The wavelength used to read RhB was 554 nm [27,35].

To identify the active species in the photocatalytic process, isopropyl

alcohol (C_3H_8O), p-benzoquinone ($C_6H_4O_2$), silver nitrate ($AgNO_3$), and disodium ethylenediaminetetraacetate (EDTA) were used as scavengers for hydroxyl radicals ($HO^{\bullet}$), superoxide radical anion ($O_2^{\bullet -}$), negative charges (e^-) and positive charges (h^+), respectively [36–38].

In the catalyst reuse tests, each powder was separated by centrifugation after the analysis and then dried. The powders were then weighed, and the ratio between the catalyst (1 mg) and the RhB solution (1 mL) was maintained. The reuse process was carried out in 4 cycles. The leaching of Fe in the samples was analyzed using high-resolution continuum-source atomic absorption spectrometry (HR-CS-AAS) ContrAA 700 (Analytik Jena).

2.4. Factorial experimental design

A statistical methodology was used to optimize the photocatalysis process. For this, a 2^k factorial design experiment was carried out to investigate the influence of some parameters on the performance of photocatalysis. In a 2^k factorial design, k factors are varied on 2 levels, called low and high (-1 and + 1). In this study, the influence of four main variables was investigated: catalyst used (A) – Nb_2O_5 and 1 % Fe-Nb_2O_5, amount of catalyst in mg (B) – 25 mg and 50 mg, pH of the solution (C) – 5 and 10, and the processing time in min (D) – 30 min and 60 min, totaling 16 experiments. The discoloration value (in %) of RhB was considered a response. Table 1 presents the relationship between the variables studied and the levels.

3. Results and discussion

Fig. 1 shows the diffractogram of the pure Nb_2O_5 and Fe-Nb_2O_5 samples. Both samples show the same behavior in the diffractogram, which is related to the low crystallinity of the pseudohexagonal phase (TT) according to the crystallographic card JCPDS No. 28–0317. The samples showed this low crystallinity due to the synthesis method used (MAH), which has the property of being carried out at low temperatures, making it impossible to obtain the pure TT crystalline phase, which requires a heat treatment temperature of 500 °C, as shown in other works by the author [15,25,27]. Nb_2O_5 has the property of changing the crystalline phase when the heat treatment temperature increases. Nevertheless, the presence of the nanocrystalline phase is detected in both diffractograms of the samples, as shown in Fig. 1.

The chemical composition of the samples determined by EDXA is shown in Table 2, and the EDXA spectra of each sample are shown in Fig. S1 (Supplementary Material). The results of EDXA analysis confirm that the concentrations of the impurity Fe are close to the nominal concentration.

Raman spectroscopy, Fig. 2 (a), shows the presence of the vibrational modes characteristic of Nb_2O_5. As the amount of iron increases, the intensity of the vibrational modes also increases. The mode at 678 cm^{-1} is attributed to the symmetric stretching modes of the polyhedra of NbO_6, NbO_7, and NbO_8, which are characteristic of amorphous and low-crystallinity Nb_2O_5 samples [39,40]. At 224 cm^{-1}, the presence of bending vibrations of Nb–O–Nb compounds is detected [39,41]. Moreover, the active mode at 102 cm^{-1} is associated with the integral vibration of octahedra [15,42].

Fig. 2 (b) shows the infrared spectroscopy of the samples. The peaks in the regions of 3600 and 3000 cm^{-1} are related to the adsorption of water by the material [25,43]. The peaks at 1720 cm^{-1} and 1662 cm^{-1} correspond to the angular vibrations of water molecules [25,43–45]. The peaks at 1370 and 1220 cm^{-1} can be attributed to the niobium precursor used ($(NH_4[NbO(C_2O_4)_2(H_2O)].(H_2O)n$), which may contain a residual organic component [43]. The peak at 903 cm^{-1} indicates stretching of the Nb = O bond [44]. The peak at 795 cm^{-1} is characterized by the angular deformation vibration of Nb-O-Nb, and the peak at 855 cm^{-1} corresponds to the asymmetric stretching of the O-Nb-O bonds [44,45].

Table 1
Relationship between the studied variables and levels.

Variables	Level	
	−1 (low)	+1 (high)
Sample (A)	Nb_2O_5	1 % Fe-Nb_2O_5
Nb_2O_5 dosage (mg) (B)	25	50
pH (C)	5	10
Time (min) (D)	30	60

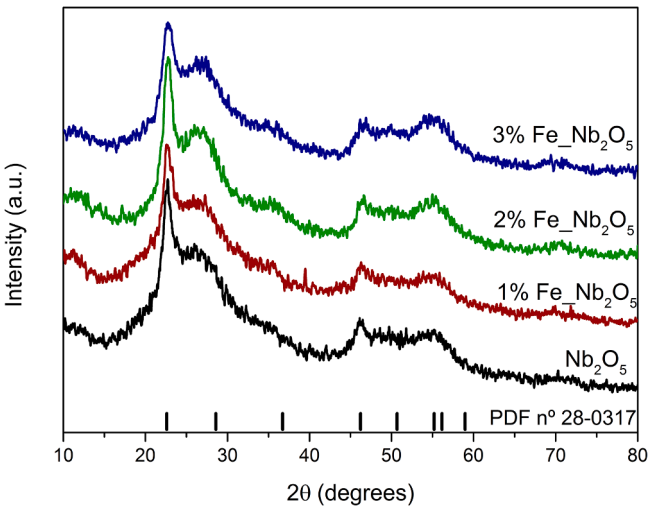

Fig. 1. Diffractogram of the samples for pure Nb_2O_5, 1% Fe-Nb_2O_5, 2% Fe-Nb_2O_5, and 3% Fe-Nb_2O_5.

Table 2
EDXA results.

Sample	Analyte	
	Nb	Fe
1 % Fe-Nb_2O_5	99.053 %	0.820 %
2 % Fe-Nb_2O_5	98.251 %	1.749 %
3 % Fe-Nb_2O_5	97.054 %	2.817 %

The SEM images of the samples are shown in Fig. 3. The Nb_2O_5 sample, as shown in other works, is very characteristic of the synthesis method and shows agglomerates of particles aggregated among themselves (Fig. 3 (a) and (b)). When 1 % Fe was inserted into Nb_2O_5 (Fig. 3 (c) and (d)), it was possible to detect the presence of pores between the particles. However, it seems that for the pure Nb_2O_5 sample, the particle agglomerates increased and became denser. In Fig. 3 (e) and (f), based on 2 % Fe-Nb_2O_5, the particles are more aggregated with each other and form large particle agglomerates, and the distances between the agglomerates are reduced to 1 % Fe-Nb_2O_5. After inserting 3 % Fe, the particles became more compact and larger than the others. This particle aggregation is very characteristic of the MAH synthesis method for Nb_2O_5, which uses a low temperature and a short synthesis time that do not favor the growth of particle size, which in turn favors particle aggregation and agglomeration. The property of the particles may affect the photocatalytic response of the material, since smaller particles with more pores favor the adsorption of the dye [46].

The TEM images are shown in Fig. 4. The pure Nb_2O_5 sample, Fig. 4 (a), shows blocky particles, which is characteristic of the sample synthesized by this synthesis method [25,47]. In the sample with Fe impurity insertion, as shown in Fig. 4 (b), the particle size was not uniform, and the samples showed a porous structure, which was consistent with the SEM images, as shown in Fig. 3.

The specific surface area (S_{BET}) of the materials was evaluated, as it is an important parameter in the photocatalytic process. For Nb_2O_5, an

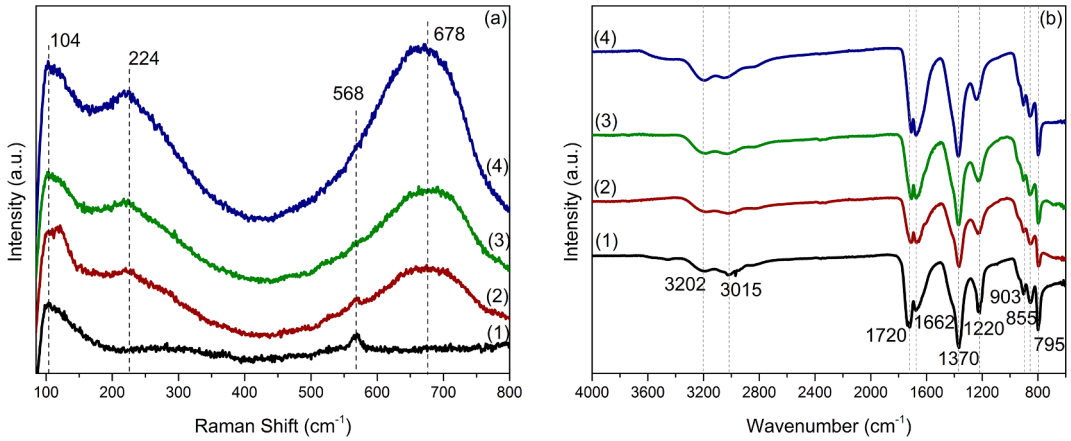

Fig. 2. (a) Raman spectroscopy of the samples, where (1) is pure Nb_2O_5, (2) 1% Fe-Nb_2O_5, (3) 2% Fe-Nb_2O_5, and (4) 3% Fe-Nb_2O_5; and (b) FTIR spectra of the samples, where (1) is pure Nb_2O_5, (2) 1% Fe-Nb_2O_5, (3) 2% Fe-Nb_2O_5, and (4) 3% Fe-Nb_2O_5.

S_{BET} of 1.453 m^2g^{-1} was found. With the increase in impurity concentration, there was an increase in S_{BET}, where 1 % Fe-Nb_2O_5 presented 1.011 m^2g^{-1}, 2 % Fe-Nb_2O_5 1.266 m^2g^{-1} and 3 % Fe-Nb_2O_5 1.396 m^2g^{-1}. For samples with higher concentrations of Fe, such as 5 and 10 %, the values tend to increase more, being 3.402 m^2g^{-1} for 5 % Fe-Nb_2O_5 and 4.171 m^2g^{-1} for 10 % Fe-Nb_2O_5. This increase in the specific surface area for an increase in the concentration of the impurity can be explained by the fact that there is no partial blockage of the Nb_2O_5 pores [10,48].

The surface charge of the nanoparticles was determined using the zeta potential. Material stability can be guaranteed when absolute values are greater than 30 mV or less than −30 mV [49,50]. The pH used in the solution to determine the zeta potential was 7. The zeta potential values for pure Nb_2O_5, 1 % Fe-Nb_2O_5, 2 % Fe-Nb_2O_5 and 3 % Fe-Nb_2O_5 were −61.04, −55.28, −64.26 and −45.18 mV, respectively. These values seem to be in agreement with those reported in the literature for a pH close to approximately 7 [51–53]. Normally Nb_2O_5 has the characteristic of presenting zero charge point close to pH 2, and negative zeta potential conditions are verified above pH 2 [52,53]. As the pH increases, the zeta potential tends to decrease even further [51,54]. When applied in photocatalytic processes involving cationic dyes, the negatively charged zeta potential favors degradation efficiency due to the high electrostatic interaction of the positively charged dye with the negatively charged catalyst [55].

The band gap values of the samples, Fig. 5, were calculated according to the *Tauc* model by the interception of the tangent line in a graph for an indirect semiconductor of $(\alpha h\nu)^{0.5}$ versus $h\nu$, where α is the absorption coefficient and $h\nu$ is the photon energy in eV [56–58]. Nb_2O_5 exhibits a band gap of 3.06 eV. When iron was inserted in Nb_2O_5, it is possible to visualize a decrease in the band gap values of the samples as the amount of iron added to the system increases, i.e., 2.81 eV for 1 % Fe-Nb_2O_5, 2.48 eV for 2 % Fe-Nb_2O_5, and 2.41 eV for 3 % Fe-Nb_2O_5. This behavior of decreasing the band gap by visualizing the redshift is due to the inclusion of Fe^{3+} in the crystalline structure of Nb_2O_5, which allows greater absorption of visible light. Moreover, with the increase in Fe concentration in the lattice, it is proven that the color of the semiconductor material changes from white to light yellow. This is due to the formation of trapping sites by the insertion of Fe ions in the Nb_2O_5 structure.

The PL spectra of pure and Fe-inserted Nb_2O_5 samples were obtained in the range of 365–800 nm, and the results are shown in Fig. 6. Two main emission peaks (490 and 535 nm) were identified in Fig. 6 in both samples, which are characteristic of the luminescence of this material. These peaks indicate that recombination occurs through the energy levels between the band gap of the material, resulting in a broadband emission. The photoluminescent capacity of materials is directly related to the recombination velocity of the e^-/h^+ pairs, indicating that the facilitation of this recombination promotes higher PL intensities [59]. The impurity can affect the photoluminescence of the material since it can promote the appearance of defects that can act as an impediment to the recombination of e^-/h^+ pairs [60]. The Fe^{3+} ions present in the sample can result in the formation of Fe^{2+} and Fe^{4+} ions by trapping the photogenerated charge pairs. Fe^{2+} and Fe^{4+} are more unstable than the Fe^{3+} ion, which has a half-filled 3d electron configuration ($3d^5$). This causes the e^-/h^+ pairs to be readily released from the Fe^{2+} and Fe^{4+} ions to the catalyst surface, which consequently favors photocatalysis [61,62]. The 1 % Fe-Nb_2O_5 sample showed the lowest luminescent intensity, indicating that insertion with 1 % Fe favored the creation of traps in the recombination of the e^-/h^+ pairs. With this reduction in the PL intensity, it is expected that the photocatalytic activity of the material will be favored, with the availability of more e^-. In the 3 % Fe-Nb_2O_5 sample, the PL intensity is higher, indicating that the higher concentration of the impurity ion can help in the origin of defects that can favor this distance in intensity. When the impurity ion concentration is higher, Fe^{3+} can act as efficient recombination centers, since the recombination rate of the photogenerated pairs will be faster, which leads to a decrease in the photocatalytic efficiency of the material [60,62–64].

XPS analysis for all samples was performed to verify the oxidation state of the species. The survey spectra of the samples are shown in Fig. 7 (a). The binding energies of Nb 3d, C 1 s and O 1 s of all samples are very similar, and the respective high-resolution XPS spectra of each sample are shown in Fig. S2 in the supplementary material. Niobium 3d spectra (figs. S2 a, d, g and j) is composed by two peaks related to spin orbitals $3d_{5/2}$ and $3d_{3/2}$. This binding energy corresponds to Nb^{5+} oxidation state according to the literature [65,66]. Fig. S2 (b, e, h and k) shows the C 1 s XPS spectra, revealing the presence of components corresponding to C═C sp^2, C—O—C and C═O bonds [66,67]. The O 1 s XPS spectra, Fig. S2 (c, f, j and l), showed the presence of two components associated with O-Nb and probably with hydroxyl groups or carbonate species [47,65,66].The XPS spectra of Fe 2p are shown on Fig. 7 and for the Fe-Nb2O5 samples two peaks located around 710 eV and 725 eV are observed, corresponding to the Fe $2p_{3/2}$ and Fe $2p_{1/2}$ levels, respectively [68,69]. For the three samples, the Fe $2p_{3/2}$ level was deconvoluted in two components, one of lower intensity located around 707.0 eV attributed to Fe^{2+} and one of high intensity located around 711 eV, attributed to Fe^{3+} [68,69]. These data indicate that both Fe^{2+} and Fe^{3+} ions are present in the Nb_2O_5 structure. In terms of iron concentration, the 1 % Fe-Nb_2O_5 sample presents the highest amount of Fe^{2+} (approximately 7.1 %), while the 3 % Fe-Nb_2O_5 sample had the lowest amount of Fe^{2+} (approximately 2.0 %), which could explain the best photocatalytic activity for the 1 % Fe-Nb_2O_5 sample attributed the higher amount of Fe^{2+} available, facilitating the release of

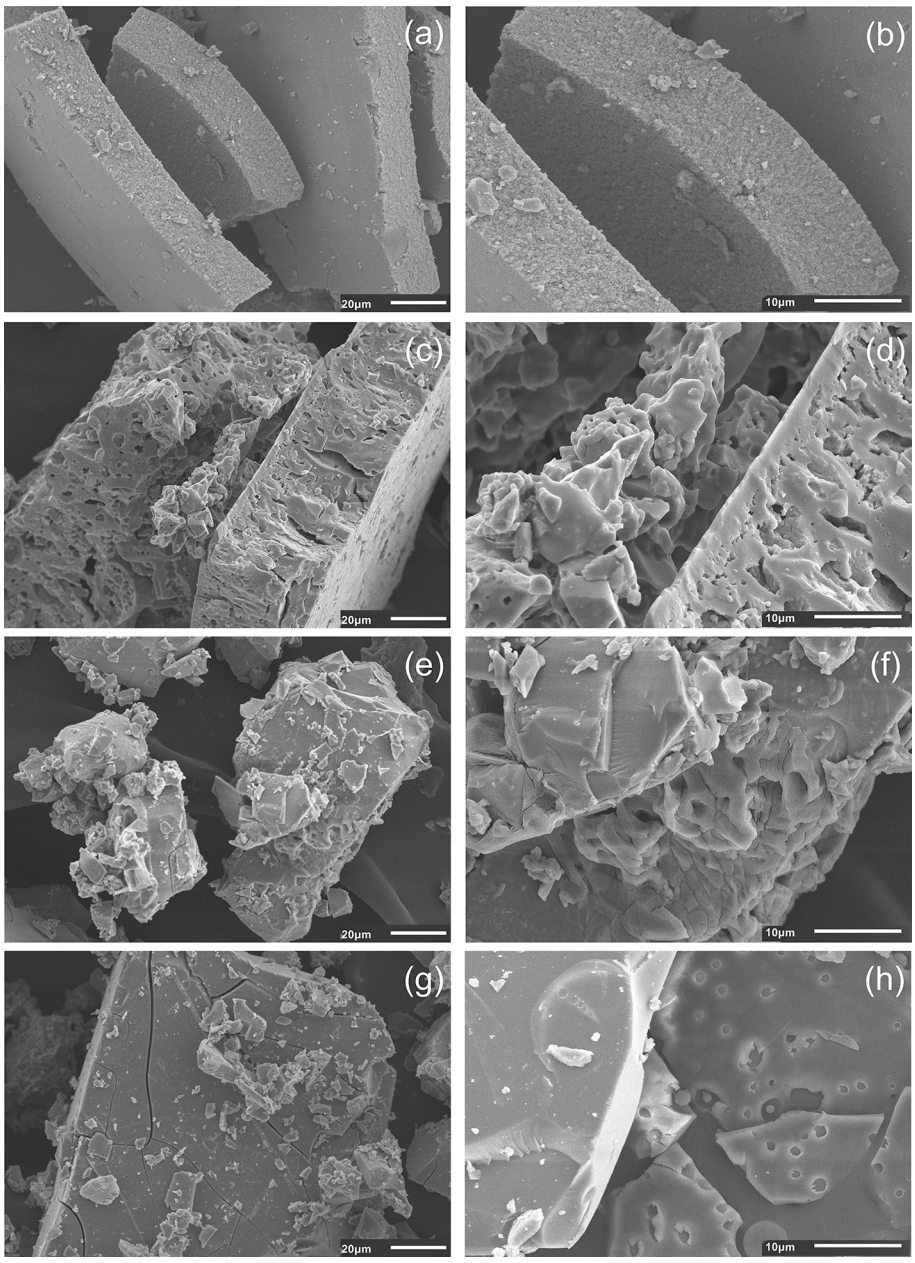

Fig. 3. Scanning electron microscopy (SEM) images of the pure and Fe-Nb_2O_5 samples, where (a) and (b) pure Nb_2O_5; (c) and (d) 1% Fe-Nb_2O_5; (e) and (f) 2% Fe-Nb_2O_5; and (g) and (h) 3% Fe-Nb_2O_5.

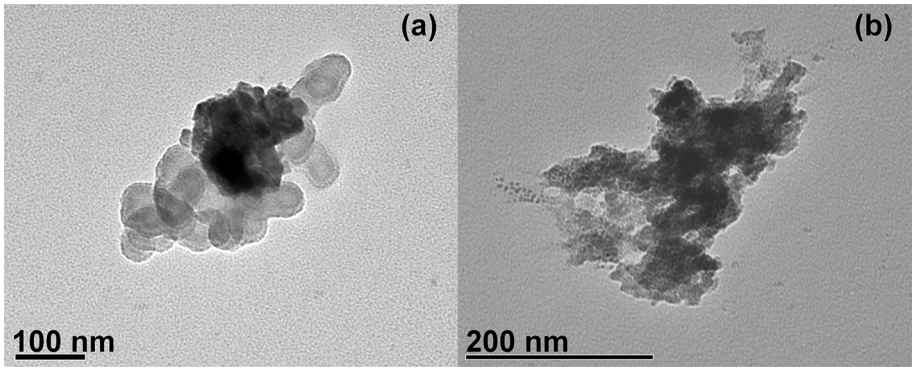

Fig. 4. TEM images, where (a) is Nb_2O_5 and (b) 1% Fe-Nb_2O_5.

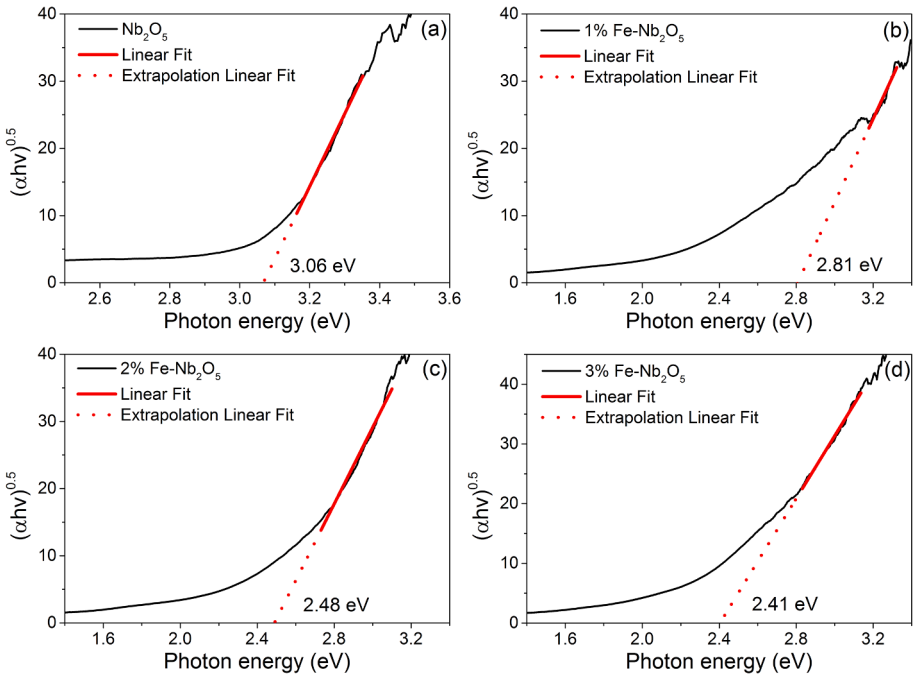

Fig. 5. Tauc plots of the samples, where (a) pure Nb_2O_5, (b) 1% Fe-Nb_2O_5, (c) 2% Fe-Nb_2O_5 and (d) 3% Fe-Nb_2O_5.

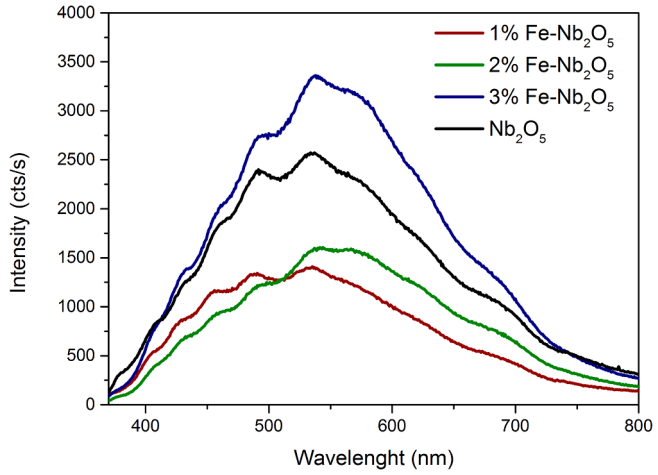

Fig. 6. PL spectra of the samples.

photogenerated pairs on the catalyst surface and favoring the photocatalysis process.

3.1. Photocatalytic activity

The photocatalytic behavior of the samples against the RhB dye and the time of 60 min under UVC irradiation is shown in Fig. 8. Fig. 8 (a) shows the photocatalytic curve of the samples every 10 min, where C_0 is the initial concentration of the solution and C is the point concentration over time. The RhB curve without a semiconductor is important to show that the photocatalyst has an important effect on the process, as it only shows a natural discoloration over time. Nb_2O_5 has the property of being a photocatalyst, as shown in other works [15,27]. It can be shown that pure Nb_2O_5 exhibits approximately 92 % discoloration within 60 min under these synthesis conditions. The samples with 1 and 2 % iron showed better and similar results to Nb_2O_5, where 1 % Fe-Nb_2O_5 was able to discolor RhB to 100 % in 60 min, while 2 % Fe-Nb_2O_5 discolored 91 %. On the other hand, 3 % Fe-Nb_2O_5 showed worse behavior than the pure Nb_2O_5 sample, which was able to decolorize 61 % of RhB.

The reaction rate constant (k) of each sample was estimated using the Langmuir-Hinshelwood kinetic model based on the linear relationship between -ln (C/C_0) and reaction time. Fig. 8 (b) follows the pseudofirst-order reaction, expressed as -ln (C/C_0) = kt, where t is the time in minutes. The k value of 1 % Fe-Nb_2O_5 has the highest value of 0.06806, followed by Nb_2O_5 with k of 0.04205, 2 % Fe-Nb_2O_5 with k of 0.03908, 3 % Fe-Nb_2O_5 with k of 0.01586, and finally RhB without catalyst with k of 0.00276. This shows that 1 % Fe-Nb_2O_5 is 1.62 times more efficient than Nb_2O_5, 1.74 times more efficient than 2 % Fe-Nb_2O_5, 4.29 times more efficient than 3 % Fe-Nb_2O_5, and 24.66 times more efficient than RhB without catalyst.

In this work, it was demonstrated that only a concentration of iron ions of 1 % showed an increase in the photocatalytic discoloration of the material. As the concentration of iron increases, the photocatalytic performance decreases. This indicates that an inserted material does not always show the best response in photocatalysis. Lower concentrations of ion insertion generally improve the photocatalytic activity of a semiconductor because the excited electrons can be trapped more efficiently, in contrast to an excess of ion insertion, which leads to faster recombination of the photogenerated electron-hole pairs and decreases the photocatalytic behavior of a given material, which was visible in the sample of 3 % Fe-Nb_2O_5.

This result corroborates the SEM and PL analyses, as shown above in Figs. 3 and 6. The 1 % Fe-Nb_2O_5 sample exhibited higher particle porosity than the other samples, which favored the best photocatalytic activity of this sample against RhB discoloration. Moreover, the same sample exhibited a lower PL intensity, which inhibited the charge recombination of the photogenerated charge pairs and consequently favored the photocatalytic activity. Additionally, it is worth mentioning that generally, the greater the surface area of the materials is, the better the photocatalytic performance will be, since there is better contact between the semiconductor surface and the dye. However, in this work, it is verified that the 1 % Fe-Nb_2O_5 sample presented the lowest S_{BET} and the best photocatalytic result, showing that despite having a lower S_{BET}, it has properties that favor the best efficiency, according to the results described above, such as SEM, XPS and PL. Some works in the literature also found this particularity of obtaining better photocatalytic performance for smaller surface areas. Raba-Páez et al. (2020) inserted

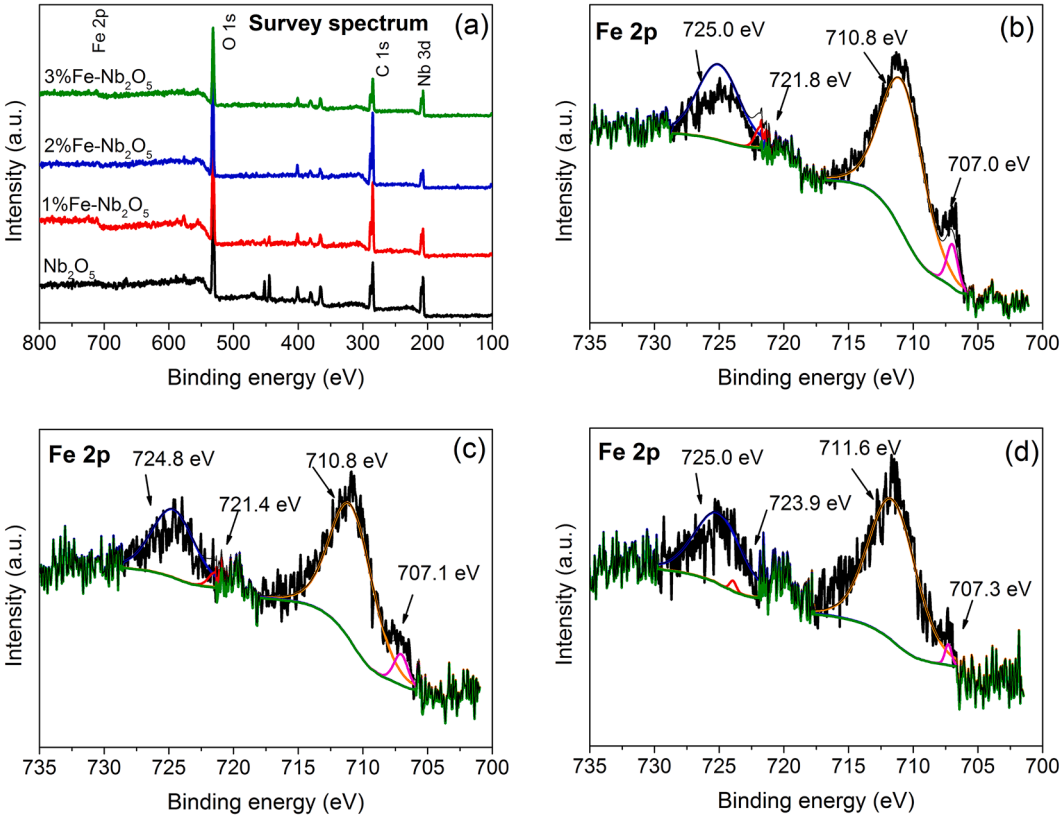

Fig. 7. XPS spectra: (a) survey, (b) HR-XPS spectra of Fe 2p for 1%Fe-Nb_2O_5, (c) HR-XPS spectra of Fe 2p for 2%Fe-Nb_2O_5, and (d) HR-XPS spectra of Fe 2p for 3% Fe-Nb_2O_5.

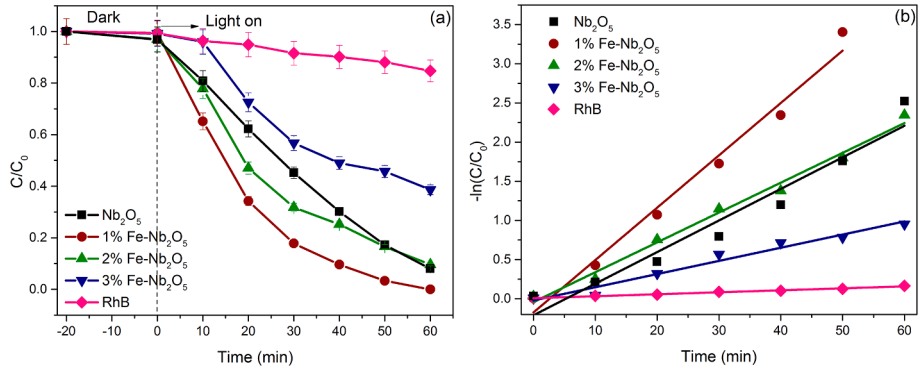

Fig. 8. (a) Concentration variation of the RhB dye for the pure and Fe-inserted Nb_2O_5 samples and (b) -ln (C/C_0) curve showing the values of pseudofirst-order rate constants (k) for the samples.

different concentrations of manganese in Nb_2O_5 (1, 2.5, 5 and 10 %) and found that with increasing Mn concentration, there was an increase in surface area and a decrease in photocatalytic performance [10]. Wang et al. (2019) subjected samples of Nb_2O_5 supported with manganese oxide to different heat treatment temperatures and found that with increasing temperature, the surface area decreased, and when applied in photocatalysis processes, the authors found that the sample with a lower S_{BET} value showed better photocatalytic performance [48].

Tests were also performed with higher Fe concentrations in Nb_2O_5, such as 5 and 10 %, which are shown in Fig. S3 of the supplementary material. As the iron concentration in the sample increases, the photocatalytic activity of the material gradually decreases, and even more so than for the 3 % Fe-Nb_2O_5 sample. In addition to the likelihood of greater recombination of charge carriers, an increased concentration of iron ions may accumulate on the surface of the catalyst, resulting in a decrease in the penetration depth of light and consequently a decrease in the performance of the material. MEV images of the 5 and 10 % materials can be seen in Fig. S4 of the supplementary material, showing an excess of iron on the surface, which justifies the decrease in performance of the materials with higher iron concentrations. In addition, the accumulation of impurities on the surface of the material may reduce the number of surface-active sites, leading to a decrease in the photocatalytic activity of the catalyst.

This behavior has been demonstrated in other works on semiconductors with various impurities. Recently, Mragui, Zegaoui, and Silva (2021) [11] showed that TiO_2 samples doped with up to 1 % cobalt exhibited better photocatalytic activity against discoloration by the dye methyl orange; a decrease in photocatalytic performance was observed at higher concentrations of the dopant. Ali et al. (2017) [70] showed the photocatalytic behavior of TiO_2 inserted with different concentrations of

iron (0, 3, 5, 7, and 10 %) against the discoloration of methylene blue in an aqueous solution under visible light illumination; the sample inserted with 3 % iron showed the best photocatalytic result, and larger amounts tended to decrease the photocatalytic capacity of the material, indicating greater charge recombination in these cases. Moradi et al. (2016) [71] also found that iron-doped TiO_2 samples at lower concentrations, such as 1 %, exhibited greater discoloration of the RR198 dye under UV irradiation and that the photocatalytic activity decreased when the Fe concentration was greater than 1 wt%.

Some studies demonstrate that the insertion of impurities in oxides such as Nb_2O_5 and TiO_2 helps to increase the photocatalytic performance. Table 3 compares the % of dye removal against these semiconductors doped with different materials. For the analysis, the best result of the impurity addition approached with the respective pure semiconductor was compared. There are few works that address the insertion of Fe dopants in Nb_2O_5 for photocatalytic applications. The efficiency obtained in this work was high, which is largely due to the use of Nb_2O_5 with low crystallinity. The works by Oliveira et al [29] and Zhang et al [72] approach the use of Nb_2O_5 with low crystallinity, showing that both have better photocatalytic performance and in less time when compared to the other crystalline phases of Nb_2O_5.

This shows that the photocatalytic performance of a particular material depends on the amount of impurity used and that a higher concentration of impurity ions does not always favor the heterogeneous photocatalysis process.

The active species in the photocatalytic process were identified by the scavenger method. Fig. 9 shows the change in RhB concentration over time using different charge scavengers. Fig. 9 (a-c) shows the performance of the pure Nb_2O_5 sample of 1 % Fe-Nb_2O_5 and 2 % Fe-Nb_2O_5. The use of EDTA, C_3H_8O and BQ as scavengers leads to a decrease in the photocatalytic efficiency of RhB in both samples, indicating that h^+, $HO^\bullet$ and $O_2^{\bullet-}$ play an important role in the desgradation of RhB. The addition of $AgNO_3$ resulted in strong adsorption of the dye in both samples but inhibited the photocatalysis of the samples. Since $AgNO_3$ suppresses e^- in the system, more h^+ is available for the process, avoiding the recombination of e^- with h^+, which favors the discoloration performance of RhB. Fig. 9 (d) shows that the addition of the EDTA and BQ scavengers slightly decreased the photocatalytic efficiency of 3 % Fe-Nb_2O_5. The addition of C_3H_8O improved the photocatalytic degradation of the sample, showing that it had a negative effect on the decolorization efficiency of the dye. This is consistent with the low performance of 3 % Fe-Nb_2O_5 in decolorizing RhB in the process (Fig. 8) to the other samples, indicating that only h^+ and $O_2^{\bullet-}$ help in the photocatalytic process.

3.2. Catalyst reusability

The reusability of the samples is shown in Fig. 10. The reusability test is important to determine the chemical stability of the material for different photocatalytic cycles. After four consecutive cycles, the samples showed a slight decrease in photocatalytic performance, which may have been related to the adsorption capacity of the dye, since reactive sites on the surface of the semiconductor material may be occupied by degradation products [74,75]. The discoloration reduction for both samples was approximately 10 %. In Table 4, it is possible to visualize the data of % RhB discoloration after 60 min of analysis, as well as the concentration of iron leaching, for cycle 1 and cycle 4 of each of the samples. These data show that the % of leaching of iron increased slightly in the fourth cycle in relation to the first for both concentrations of iron; however, even so, the value of leached Fe for the solution was relatively low, showing that the catalyst presents stability and can be used in different cycles.

3.3. Factorial design of experiments

Based on the photocatalysis data, a factorial design of experimental analysis was performed considering the pure Nb_2O_5 and the 1 % Fe-Nb_2O_5 sample to analyze the importance of ion insertion, as the 1 % Fe-Nb_2O_5 sample showed the best photocatalytic result among the ion-inserted samples. Thus, considering the use of the 2^4 factorial, Table 5 shows the data of the average of % RhB discoloration, where the combination of two levels with four variables totals 16 experiments. All experiments were performed in triplicate, and the respective results are displayed in the supplementary material, Table S1.

The individual analysis of each independent variable, as well as the combination of two, three and four variables, are important to understand the behavior and influence of each parameter on the heterogeneous photocatalysis response through the RhB discoloration. Among the 16 experiments of the factorial design of experiments, one is used as a basis for changing levels, and the other experiments are effects of the four variables existing in the process (A, B, C and D), in addition to the combination of two (AB, AC, AD, BC, BD and CD), three (ABC, ABD, ACD and BCD), and four variables (ABCD), totaling 15 different effects.

A table is provided in the supplementary material (Table S2) that shows the signs (positive and negative) for the effects in planning 2^4. To estimate the effects of interest in a factorial design, the high (+1) and low (-1) levels of each column must be taken into account, as already demonstrated in other works [15,16].

Table 6 presents the data from the ANOVA, which is used to visualize the effect of each parameter. The F *test* is a tabulated value of 7.50 (f0.01,1,32) for this work, considering a confidence interval of 99 %. To

Table 3
Comparison of the % dye degradation over samples doped with different materials.

Sample	Phase	Dye	Light	Time (min)	% RhB removal	Ref.
Nb_2O_5	Low crystallinity	RhB	UVC	60	90	This work
1 %Fe-Nb_2O_5					100	
Nb_2O_5	Orthorhombic	RhB	Vis	150	~70	[64]
3 %Fe- Nb_2O_5					98.4	
Nb_2O_5	Orthorhombic	RhB	UV	120	~15	[10]
2.5 %Mn-Nb_2O_5					~13	
Nb_2O_5	Low crystallinity	RhB	UV	180	~50	[29]
0.1 %Zn-Nb_2O_5					~90	
Nb_2O_5	Pseudohexagonal	RhB	Vis	40	~27	[73]
C-Nb_2O_5-200					100	
Nb_2O_5	Low crystallinity	Triclosan	Vis	15	100	[72]
TiO_2	Anatase	MB	Vis	90	~35	[70]
3 %Fe-TiO_2					~75	
TiO_2	Anatase	MO	Vis	360	~15	[11]
1 %Co-TiO_2					~35	
g-C_3N_4	Hexagonal	RhB	Vis	60	~60	[9]
3 %Fe-g-C_3N_4					~85	

RhB: rhodamine B; MB: methylene blue; MO: methyl orange.

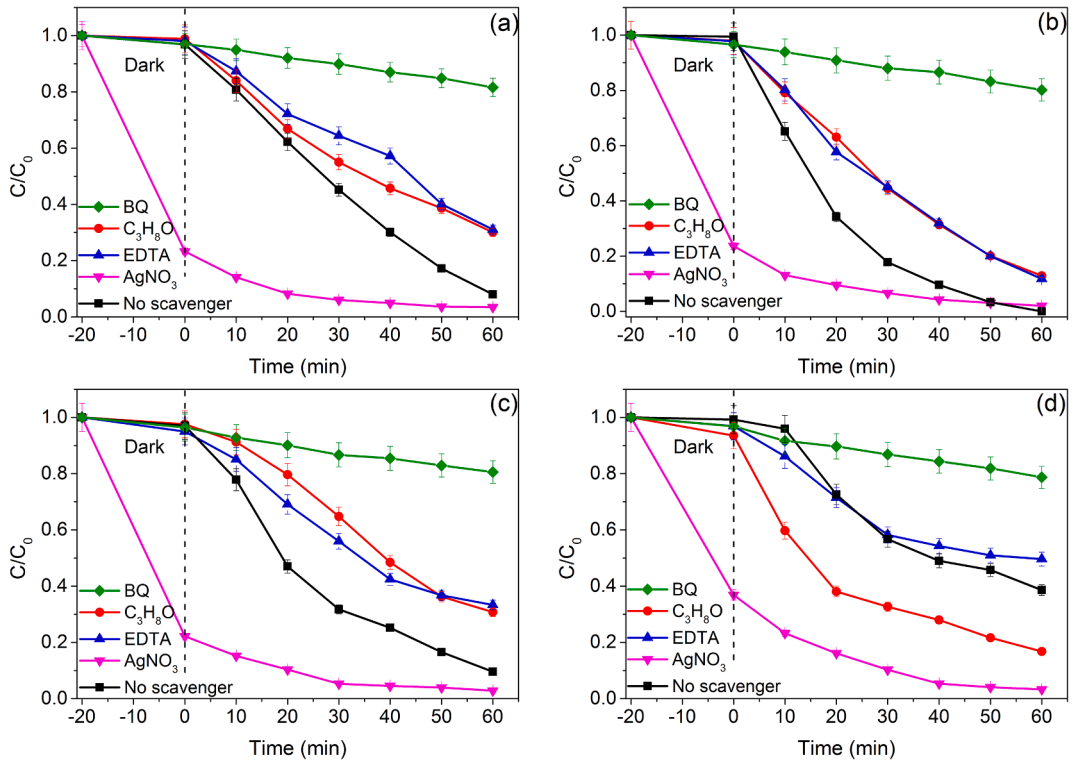

Fig. 9. Variation curves of RhB dye using the scavengers p-benzoquinone (BQ), isopropyl alcohol (C_3H_8O), silver nitrate ($AgNO_3$), and EDTA compared to the curves without scavengers for (a) Nb_2O_5, (b) 1% Fe-Nb_2O_5, (c) 2% Fe-Nb_2O_5 and (d) 3% Fe-Nb_2O_5.

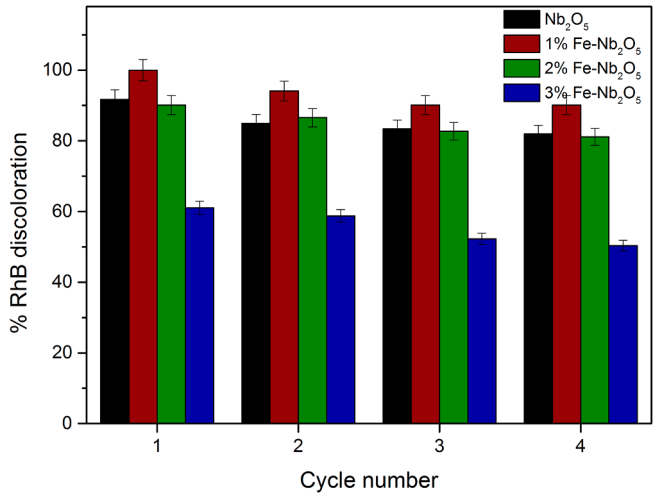

Fig. 10. Reusability of samples for 4 cycles.

evaluate the effects, a comparison was made between the values of f_0 found and with the tabulated value of the F *test* (7.50). The values of f_0 that exceeded the value of the F *test* are significant for the process, meaning that they have an influence on the variation analysed, while the values of f_0 smaller than 7.50 are not considered significant in the process. Based on the values of f_0, it is possible to analyze which variables and their interactions influenced the photocatalytic degradation process.

The calculated effect, as shown in Table 6, is used to verify whether the photocatalytic discoloration of RhB was positively significant or negatively significant, according to each parameter and interaction. All values that have a positive sign effect are positively relevant in the photocatalysis process, indicating that changing this parameter helps to obtain better photocatalytic results. The responses that showed an effect with a negative sign indicate that the alteration of this parameter somehow impairs the response of the photocatalytic process, indicating that they are negatively relevant to the photocatalysis process. A relationship between the interactions of the parameters with the value of f_0, already considering the sign of the effect, is shown in Fig. 11. Fig. 11 (a) is an overview of the values of f_0, while Fig. 11 (b) approximates Fig. 11 (a), where it is possible to verify that all f_0 values that exceeded the blue color line were significant for the photocatalytic process. From Fig. 11, it is noted that of 16 independent experiments, at a confidence interval of 99 %, 12 had a significant influence on the process due to the values of f_0 being greater than the F *test* (7.50).

Variable A, which indicates the change from the sample of Nb_2O_5 to the sample of 1 % Fe-Nb_2O_5, presented the most expressive value of f_0,

Table 4
Summary of RhB discoloration results, AAS and Fe leached values for cycle 1 and cycle 4 of the photocatalytic analysis.

Sample	RhB removal 1st (%)	RhB removal 4th (%)	*Fe 1st (mg/L)	*Fe 4th (mg/L)	**Fe leaching 1st (%)	**Fe leaching 4th (%)
1 %Fe Nb_2O_5	100	90.10	0.414	0.465	0.828	0.93
2 %Fe-Nb_2O_5	90.12	81.11	0.580	0.599	0.58	0.6
3 %Fe-Nb_2O_5	61.06	50.36	0.764	1.008	0.51	0.672

* Fe determined in the aqueous phase by atomic absorption spectrometry.
** Fe leached after the 1st and 4th photocatalytic cycles in relation to the initial Fe composition in the catalysts.

Table 5
Average RhB removal (%) for a factorial design 2^4 with variable values for 16 experiments.

Experiment	A	B	C	D	Parameter interaction	Average RhB removal (%)	Effects
1	−1	−1	−1	−1	1	51.36	39.02
2	1	−1	−1	−1	A	84.81	−2.44
3	−1	1	−1	−1	B	54.52	−3.28
4	1	1	−1	−1	AB	80.12	−23.91
5	−1	−1	1	−1	C	21.02	19.57
6	1	−1	1	−1	AC	84.71	−4.37
7	−1	1	1	−1	BC	18.48	−0.09
8	1	1	1	−1	ABC	71.92	20.97
9	−1	−1	−1	1	D	85.67	−5.02
10	1	−1	−1	1	AD	97.51	1.78
11	−1	1	−1	1	BD	92.76	1.24
12	1	1	−1	1	ABD	99.69	−5.23
13	−1	−1	1	1	CD	37.63	5.05
14	1	−1	1	1	ACD	97.86	−0.92
15	−1	1	1	1	BCD	33.29	0.51
16	1	1	1	1	ABCD	90.28	39.02

Table 6
ANOVA table for the model obtained for % RhB discoloration.

Source of Variation	Sum of Squares	Degrees of Freedom	Mean Square	f_0	*F test*
A	18271.36	1	18271.364	7513.4	7.50
B	71.53	1	71.526135	29.4124	7.50
C	6857.66	1	6857.6642	2819.95	7.50
D	5275.77	1	5275.7744	2169.46	7.50
AB	129.36	1	129.36117	53.1948	7.50
AC	4594.63	1	4594.6333	1889.37	7.50
AD	302.75	1	302.7549	124.496	7.50
BC	229.49	1	229.49268	94.37	7.50
BD	37.95	1	37.953119	15.6068	7.50
CD	328.64	1	328.64098	135.141	7.50
ABC	0.10	1	0.1019677	0.04193	7.50
ABD	18.56	1	18.560332	7.63222	7.50
ACD	305.46	1	305.46365	125.61	7.50
BCD	10.23	1	10.228761	4.20618	7.50
ABCD	3.07	1	3.0744158	1.26424	7.50
Error	**77.82**	**32**	**2.43**		
Total	**36514.41**	**47**			

with a positive effect, indicating that the sample with 1 % Fe greatly improves the photocatalytic response. This is very clear in Fig. 8, where the Fe-inserted sample shows a discoloration of 82 % in 30 min of analysis, while the pure Nb_2O_5 sample discolored 55 % in 30 min. All level changes for parameter A shows better efficiencies. This has been explained before, where small amounts of ions added to the system improve electron capture.

Variable B also presented a f_0 greater than 7.50, but with a negative effect, indicating that the change in the amount of catalyst, from 25 mg to 50 mg, impairs the photocatalytic process, decreasing the discoloration response of RhB. This show that the use of a smaller amount of catalyst in the process, in addition to presenting better results of RhB discoloration, generates savings in the process, since it is possible to use half the amount of sample. Generally, a greater amount of catalyst contributes to the presence of more active sites on the surface, which favors the photocatalytic process [76,77]. However, under the conditions of this work, it was found that a smaller amount of material can decolorize RhB more effectively than larger amounts. This can be explained by saturation of the amount, causing the solution to become cloudy and consequently lose its ability to decolorize RhB.

Changing only the variable C greatly impairs the photocatalytic performance, since the change in this variable presented a much higher f_0 than the F *test* and had a negative effect. This variable refers to the pH change of the sample. This indicates that the acidic RhB solution (pH 5) has a greater decolorization capacity under the conditions of this work, indicating that H^+ present in the solution helps to improve photocatalytic degradation through the interaction with the oxidizing species that are responsible for the oxidation of the cationic dye, that is, RhB [78]. Under alkaline conditions, where there is deprotonation of the –COOH group, photocatalytic degradation tends to decrease. Additionally, the point of zero charge of Nb_2O_5 is in acidic conditions, thus making the values of zeta potentials that are closer to the point of zero charge tend to present better photoactivity [54].

The variable D has a positive effect and a much higher f_0 than the F *test*. This shows that the time of the photocatalytic process influences the discoloration response of RhB. This significant improvement in the process is clearly confirmed by the results found, as shown in Table 5, where the change in variable D reached higher percentages of RhB discoloration. The increase in time tends to increase the adsorption of a material through processes of mass transfer and diffusion in solution [79]. For the conditions of this work, this variable showed an improvement in photocatalysis for the time of 60 min, indicating that there was no saturation of the photocatalyst, indicating that there are still active sites in the material that help this condition of photocatalytic performance.

In the interactions between two parameters, different results were visualized. The AB interaction presented a f_0 greater than 7.50 and had a negative effect. In this experiment, even with a very significant variable A, the interaction of A with B had a negative effect on the process, indicating that when there was a simultaneous change in the catalyst and the amount of the respective catalyst, the photocatalytic response tends to decrease.

The AC interaction has a positive effect, with f_0 much higher than 7.50, as shown in Table 6, indicating that the sample inserted with Fe together with pH 10 favors an increase in the photocatalytic activity of the process. Even though the variable C alone has a negative effect, the interaction between AC proved to be positive for the process.

The interaction between AD is negatively significant to the process.

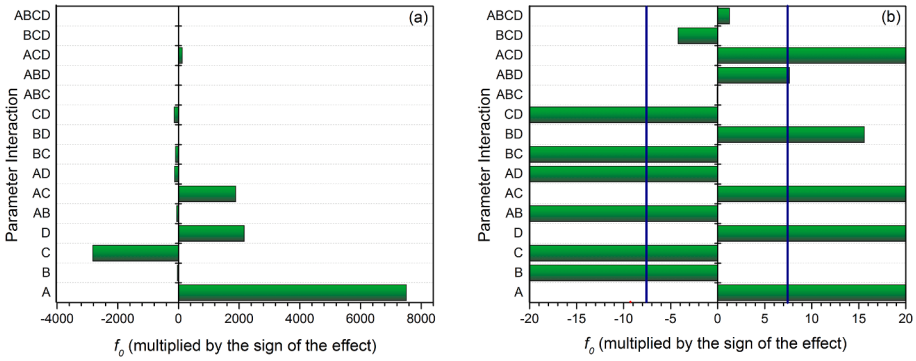

Fig. 11. (a) Relation of f_0 with the sign of the effect and (b) approximation of (a) with the delimitation of the F *test* (7.50).

This result is interesting, where even though variables A and D individually show a significant improvement in photocatalysis, the interaction between these two parameters has a negative influence. This result could be explained by the excellent degradation result obtained in A, where more than 80 % of degradation has already been reached; logically, the degradation index in the last 30 min was lower.

Additionally, considering the two interactions, the BC interactions (catalyst dosage and pH) and CD (pH and time) negatively influence the process, while the BD interaction (dosage and time) positively influences the photocatalytic performance. The interaction between three variables, ABD and ACD, also had a significant positive influence on the photocatalytic process. The ABC, BCD and ABCD interactions had no significant influence on the photocatalytic discoloration of RhB in this work.

Response surface analysis was performed to evaluate the interaction between the variables on the results obtained in a more effective way, as shown in Fig. 12. Response surface graphs were plotted for each of the catalysts (Nb_2O_5 and 1 % Fe-Nb_2O_5), fixing at each moment a variable. Through ANOVA, the variables that presented greater significance in the process were considered, with variable B fixed at 25 mg, variable C fixed at pH 5 and variable D at 60 min. Fig. 10 (a), for the sample of Nb_2O_5 fixing the variable B, verifies that the use of pH 10 drastically decreases the photocatalytic performance, and with the increase in the reaction time, there is an increase in the response of % of discoloration of rhodamine B. With fixed variable C (Fig. 12 (b)) considering the Nb_2O_5 sample, it is verified that there is a performance gain with the increase in the analysis time and that with the catalyst dosage, there are no major changes. Fixing the time parameter (variable D), Fig. 12 (c) shows that the use of pH 10 greatly decreases the % discoloration of RhB but increasing the dosage does not provide major changes in the photocatalytic process.

When the catalyst material changes from Nb_2O_5 to 1 % Fe-Nb_2O_5 (Fig. 12 (d-f)), the first check is in relation to the amount of rhodamine B discolored in the process over time, according to % values. In Fig. 12 (d),

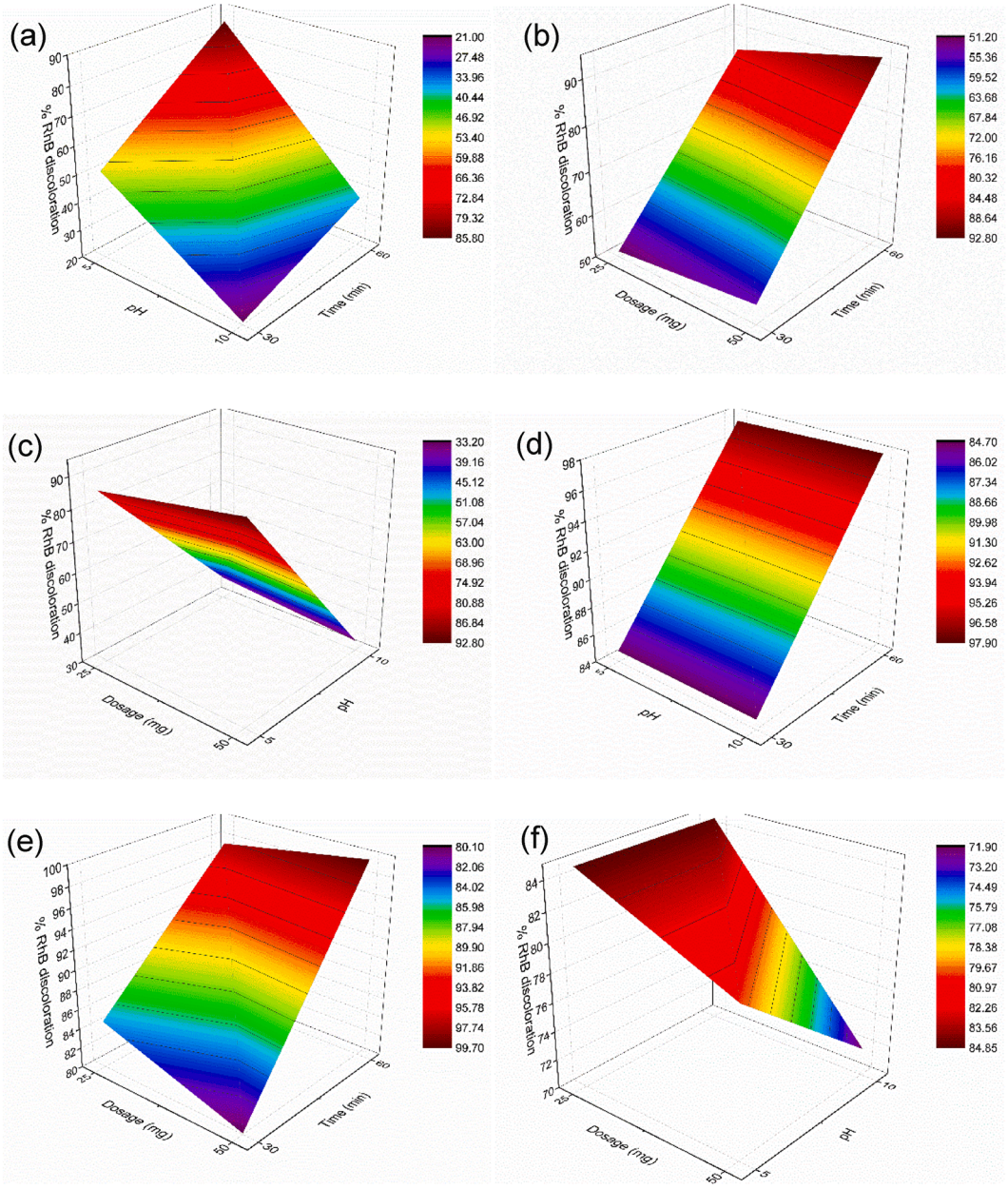

Fig. 12. (a) Nb_2O_5, dosage 25 mg; (b) Nb_2O_5, pH 10; (c) Nb_2O_5, time 60 min, (d) 1 % Fe-Nb_2O_5, dosage 25 mg; (b) 1 % Fe-Nb_2O_5, pH 10; (c) 1 % Fe-Nb_2O_5, time 60 min.

the change in pH alone does not significantly change the result, while the change in time greatly increases the photocatalytic performance of the material. The fixation of variable C, as shown in Fig. 12 (e), also shows that increasing the process time increases the photocatalytic response of the material. Fig. 12 (f) shows the 1 % Fe-Nb_2O_5 sample with the fixed time variable, where increasing the dosage from 25 to 50 mg decreases the % discoloration of RhB at both pH values. Additionally, the increase in the pH value of the solution, considering the same catalyst dosage, decreases for the highest dosage and remains at 25 mg.

4. Conclusion

Obtaining Nb_2O_5 by the MAH method is easy, fast and requires low temperatures. Iron ion insertion was performed effectively, showing a strong effect on the microscopic, surface, and optical properties of Nb_2O_5. XRD showed the presence of Nb_2O_5 with low crystallinity of the pseudohexagonal phase, which is characteristic, due to the low synthesis temperature. The SEM images showed that the incorporation of Fe into the niobium structure causes porosity in Nb_2O_5 and that as the concentration of the Fe ion increases, Fe saturation is observed on the surface of the material. The band gap of the inserted samples decreases in relation to pure Nb_2O_5 as the Fe concentration increases.

In the heterogeneous photocatalysis, the 1 % Fe-Nb_2O_5 sample showed a better result of discoloration of RhB compared with the other samples, being able to decolor 100 % of the RhB dye in 60 min of analysis. As the Fe concentration increases, a decrease in the photocatalytic performance is noticed due to the increase in charge recombination. In the 2^4 factorial design, performed for the pure sample compared to the sample with the best performance (1 % Fe-Nb_2O_5), 4 different variables were evaluated, as well as their interactions. The catalyst (A), catalyst dosage (B), pH (C) and reaction time (D) had a significant effect on the process, with A and D being positive and B and C being negative, as well as the interactions between the variables. Often, the variables alone present a positive performance, and when they interact with other variables, there may be a drop in the efficiency of the process, or vice versa, showing the importance of carrying out a statistical study to evaluate all the variables that influence or can influence the photocatalytic activity. These results help in choosing the photocatalytic routes to be followed, making it possible to discard analyses that show a drop in photocatalytic efficiency, generating savings in analysis time and materials to be used.

CRediT authorship contribution statement

Cátia Liane Ücker: Conceptualization, Methodology, Software, Investigation, Writing – Original Draft. **Vitor Goetzke:** Formal analysis, Investigation, Data curation. **Fábio Calcagno Riemke:** Methodology, Software. **Marcely Echeverria Oliveira:** Formal analysis. **Neftali Lenin Villarreal Carreno:** Resources, Formal analysis. **Fernando Dal Pont Morisso:** Formal analysis. **Marcio Daldin Teodoro:** Formal analysis, Writing – Review & Editing. **Valmor R. Mastelaro:** Formal analysis, Writing – Review & Editing. **Mário Lúcio Moreira:** Writing – Review & Editing, Supervision. **Cristiane Wienke Raubach:** Writing – Review & Editing, Supervision. **Sergio da Silva Cava:** Writing – Review & Editing, Supervision, Project administration.

Declaration of Competing Interest

The authors declare that they have no known competing financial interests or personal relationships that could have appeared to influence the work reported in this paper.

Data availability

Data will be made available on request.

Acknowledgments

The authors are thankful for the financial support of Brazilian research financing institutions: CAPES, CNPq, FAPESP (Process 2013/07296-20) and FAPERGS – Process n° 17/25510000889-8 and 19/2551-0001974-2. This study was financed in part by the Coordenação de Aperfeiçoamento de Pessoal de Nível Superior–Brasil (CAPES) – Finance Code 001. The publication of this paper was partially supported by PRPPG/UFPel. The authors would like to thank the Centro Integrado de Análises - CIA-FURG (funded by Finep-CT-INFRA, CAPES-Pró-Equipamentos, and MCTI-CNPq-SisNano2.0) for the analysis performed. The Companhia Brasileira de Metalurgia e Mineração (CBMM) is acknowledged for supplying the niobium precursor.

Appendix A. Supplementary data

Supplementary data to this article can be found online at https://doi.org/10.1016/j.jphotochem.2022.114294.

References

[1] B. Boruah, R. Gupta, J.M. Modak, G. Madras, Enhanced photocatalysis and bacterial inhibition in Nb2O5: Via versatile doping with metals (Sr, Y, Zr, and Ag): A critical assessment, Nanoscale Adv. 1 (2019) 2748–2760, https://doi.org/10.1039/c9na00305c.

[2] M. Abdi, V. Mahdikhah, S. Sheibani, Visible light photocatalytic performance of La-Fe co-doped SrTiO3 perovskite powder, Opt. Mater. (Amst). 102 (2020), 109803, https://doi.org/10.1016/j.optmat.2020.109803.

[3] C.W. Raubach, L. Polastro, M.M. Ferrer, A. Perrin, C. Perrin, A.R. Albuquerque, P. G.C. Buzolin, J.R. Sambrano, Y.B.V. de Santana, J.A. Varela, E. Longo, Influence of solvent on the morphology and photocatalytic properties of ZnS decorated CeO2 nanoparticles, J. Appl. Phys. 115 (21) (2014) 213514.

[4] J.O. Carneiro, S. Azevedo, F. Fernandes, E. Freitas, M. Pereira, C.J. Tavares, S. Lanceros-Méndez, V. Teixeira, Synthesis of iron-doped TiO2 nanoparticles by ball-milling process: The influence of process parameters on the structural, optical, magnetic, and photocatalytic properties, J. Mater. Sci. 49 (2014) 7476–7488, https://doi.org/10.1007/s10853-014-8453-3.

[5] R.D. Chekuri, S.R. Tirukkovalluri, Synthesis of cobalt doped titania nano material assisted by gemini surfactant: Characterization and application in degradation of Acid Red under visible light irradiation, South African, J Chem. Eng. 24 (2017) 183–195, https://doi.org/10.1016/j.sajce.2017.10.001.

[6] A.M. Ferrari-Lima, R.G. Marques, M.L. Gimenes, N.R.C. Fernandes-Machado, Synthesis, characterisation and photocatalytic activity of N-doped TiO2-Nb2O5 mixed oxides, Catal. Today. 254 (2015) 119–128, https://doi.org/10.1016/j.cattod.2015.02.031.

[7] K. Su, H. Liu, Z. Gao, P. Fornasiero, F. Wang, Nb2O5-Based Photocatalysts, Adv. Sci. 2003156 (2021) 1–25, https://doi.org/10.1002/advs.202003156.

[8] E.C. Paris, J.O.D. Malafatti, C.R. Sciena, L.F.N. Junior, A. Zenatti, M.T. Escote, A. J. Moreira, G.P.G. Freschi, Nb2O5 nanoparticles decorated with magnetic ferrites for wastewater photocatalytic remediation, Environ. Sci. Pollut. Res. 28 (19) (2021) 23731–23741.

[9] M.N. Van, O.L.T. Mai, C.P. Do, H.L. Thi, C.P. Manh, H.N. Manh, D.P. Thi, B., Do Danh, Fe-doped g-c3n4: High-performance photocatalysts in rhodamine b decomposition, Polymers (Basel) 12 (2020) 1–13, https://doi.org/10.3390/polym12091963.

[10] A.M. Raba-Paéz, C. Falcony-Guajardo, I. Supelano-García, M.R. Joya, Niobium pentoxide samples with addition of manganese at different concentrations and calcination temperatures applied in the photocatalytic degradation of rhodamine B, Appl. Sci. 10 (2020) 1–14, https://doi.org/10.3390/app10124257.

[11] A. El Mragui, O. Zegaoui, J.C.G. Esteves da Silva, Elucidation of the photocatalytic degradation mechanism of an azo dye under visible light in the presence of cobalt doped TiO2 nanomaterials, Chemosphere. 266 (2021), 128931, https://doi.org/10.1016/j.chemosphere.2020.128931.

[12] N.P.F. Gonçalves, M.C. Paganini, P. Armillotta, E. Cerrato, P. Calza, The effect of cobalt doping on the efficiency of semiconductor oxides in the photocatalytic water remediation, J. Environ. Chem. Eng. 7 (6) (2019) 103475.

[13] P. Jiang, W. Xiang, J. Kuang, W. Liu, W. Cao, Effect of cobalt doping on the electronic, optical and photocatalytic properties of TiO2, Solid State Sci. 46 (2015) 27–32, https://doi.org/10.1016/j.solidstatesciences.2015.05.007.

[14] M.R.D. Khaki, M.S. Shafeeyan, A.A.A. Raman, W.M.A.W. Daud, Application of doped photocatalysts for organic pollutant degradation - A review, J. Environ. Manage. 198 (2017) 78–94, https://doi.org/10.1016/j.jenvman.2017.04.099.

[15] C.L. Ücker, V. Goetzke, S.R. Almeida, E.C. Moreira, M.M. Ferrer, P.L.G. Jardim, M. L. Moreira, C.W. Raubach, S. Cava, Photocatalytic degradation of rhodamine B using Nb2O5 synthesized with different niobium precursors: Factorial design of experiments, Ceram. Int. 47 (2021) 20570–20578, https://doi.org/10.1016/j.ceramint.2021.04.066.

[16] V. Goetzke, C.L. Ücker, L.T. Gularte, C.D. Fernandes, M.L. Moreira, S. da Silva Cava, P.L.G. Jardim, R. Camaratta, C.W. Raubach, A Statistical Study of Assembly Parameter Modifications Effects on the Photovoltaic Response of Dye-Sensitized

Solar Cells, J. Electron. Mater. 50 (2021) 6149–6158, https://doi.org/10.1007/s11664-021-09136-8.
[17] T.L. Valerio, G. Tractz, G.A. Rodrigues Maia, E.d.P. Banczek, P.R. Pinto Rodrigues, Minimizing of charge recombination by Nb2O5 addition in dye-sensitized solar cells, Opt. Mater. (Amst). 109 (2020) 110310.
[18] A. Mirzaei, G.J. Sun, J.K. Lee, C. Lee, S. Choi, H.W. Kim, Hydrogen sensing properties and mechanism of NiO-Nb2O5 composite nanoparticle-based electrical gas sensors, Ceram. Int. 43 (2017) 5247–5254, https://doi.org/10.1016/j.ceramint.2017.01.050.
[19] A.S. Mokrushin, T.L. Simonenko, N.P. Simonenko, P.Y. Gorobtsov, N.C. Kadyrov, E. P. Simonenko, V.G. Sevastyanov, N.T. Kuznetsov, Chemoresistive gas-sensing properties of highly dispersed Nb2O5 obtained by programmable precipitation, J. Alloys Compd. 868 (2021) 159090.
[20] F.C. Riemke, C.L. Ücker, N.L.V. Carreño, S. da Silva Cava, M.P. Teixeira, H. V. Fajardo, J.G. Taylor, M.J. da Silva, D.C. Batalha, C.W. Raubach, Influence of Nb2O5 grown on SrTiO3 nanoseeds in the catalytic oxidation of thioanisole, Mater. Chem. Phys. 278 (2022) 125591.
[21] K. Razmgar, M. Altarawneh, I. Oluwoye, G. Senanayake, Ceria-supported niobium oxide catalyst for low-temperature oxidation of 1,3-butadiene, Mol. Catal. 518 (2022), 112083, https://doi.org/10.1016/j.mcat.2021.112083.
[22] A.K. Kulkarni, R.P. Panmand, Y.A. Sethi, S.R. Kadam, S.P. Tekale, G. Baeg, A. V. Ghule, B.B. Kale, In situ preparation of N doped orthorhombic Nb2O5 nanoplates / rGO composites for photocatalytic hydrogen generation under sunlight, Int. J. Hydrogen Energy. 43 (2018) 19873–19884, https://doi.org/10.1016/j.ijhydene.2018.09.013.
[23] O.F. Lopes, V.R. De Mendonça, F.B.F. Silva, E.C. Paris, C. Ribeiro, Óxidos de Nióbio: Uma visão sobre a síntese do Nb2O5 e sua aplicação em Fotocatálise Heterogênea, Quim. Nova. 38 (2015) 106–117, https://doi.org/10.1590/S0100-40422010000800018.
[24] C.L. Ücker, V. Goetzke, F.C. Riemke, M.L. Vitale, L.R.Q. de Andrade, M.D. Ücker, E. C. Moreira, M.L. Moreira, C.W. Raubach, S.S. Cava, Multi-Photonic behavior of Nb2O5 and its correlation with synthetic methods, J. Mater. Sci. 56 (2021) 7889–7905, https://doi.org/10.1007/s10853-021-05770-z.
[25] C.L. Ücker, L.T. Gularte, C.D. Fernandes, V. Goetzke, E. Ceretta, C.W. Raubach, M. L. Moreira, S.S. Cava, Investigation of the properties of niobium pentoxide for use in dye-sensitized solar cells, J. Am. Ceram. Soc. 102 (2019) 1884–1892, https://doi.org/10.1111/jace.16080.
[26] C.R. Strauss, D.W. Rooney, Accounting for clean, fast and high yielding reactions under microwave conditions, Green Chem. 12 (2010) 1340–1344, https://doi.org/10.1039/c0gc00024h.
[27] C.L. Ücker, F.C. Riemke, N.F. de Andrade Neto, A.d.A.G. Santiago, T. J. Siebeneichler, N.L.V. Carreño, M.L. Moreira, C.W. Raubach, S. Cava, Influence of Nb2O5 crystal structure on photocatalytic efficiency, Chem. Phys. Lett. 764 (2021) 138271.
[28] G. Falk, M. Borlaf, M.J. López-Munoz, J.C. Fariñas, J.B.R. Neto, R. Moreno, Microwave-assisted synthesis of Nb2O5 for photocatalytic application of nanopowders and thin films, J. Mater. Res. 32 (2017) 3271–3278, https://doi.org/10.1557/jmr.2017.93.
[29] J.A. Oliveira, M.O. Reis, M.S. Pires, L.A.M. Ruotolo, T.C. Ramalho, C.R. Oliveira, L. C.T. Lacerda, F.G.E. Nogueira, Zn-doped Nb 2 O 5 photocatalysts driven by visible-light: An experimental and theoretical study, Mater. Chem. Phys. 228 (2019) 160–167, https://doi.org/10.1016/j.matchemphys.2019.02.062.
[30] C.R. Shyniya, K.A. Bhabu, T.R. Rajasekaran, Enhanced electrochemical behavior of novel acceptor doped titanium dioxide catalysts for photocatalytic applications, J. Mater. Sci. Mater. Electron. 28 (2017) 6959–6970, https://doi.org/10.1007/s10854-017-6396-6.
[31] J. Chen, H. Wang, G. Huang, Z. Zhang, L. Han, W. Song, M. Li, Y. Zhang, Facile synthesis of urchin-like hierarchical Nb 2 O 5 nanospheres with enhanced visible light photocatalytic activity, J. Alloys Compd. 728 (2017) 19–28, https://doi.org/10.1016/j.jallcom.2017.08.266.
[32] A.W. Skinner, A.M. DiBernardo, A.M. Masud, N. Aich, A.H. Pinto, Factorial design of experiments for optimization of photocatalytic degradation of tartrazine by zinc oxide (ZnO) nanorods with different aspect ratios, J. Environ. Chem. Eng. 8 (5) (2020) 104235.
[33] A. Elhalil, H. Tounsadi, R. Elmoubarki, F.Z. Mahjoubi, M. Farnane, M. Sadiq, M. Abdennouri, S. Qourzal, N. Barka, Factorial experimental design for the optimization of catalytic degradation of malachite green dye in aqueous solution by Fenton process, Water Resour. Ind. 15 (2016) 41–48, https://doi.org/10.1016/j.wri.2016.07.002.
[34] I.L.O. Brasileiro, V.S. Madeira, C.P. de Souza, A.L. Lopes-Moriyama, M.L.R. de A., Ramalho, α-Fe2O3/Nb2O5 mixed oxide active for the photodegradation of organic contaminant in water: Factorial experimental design application and reaction mechanism investigation, J. Photochem. Photobiol. A Chem. 388 (2020), 112199, https://doi.org/10.1016/j.jphotochem.2019.112199.
[35] S. Yang, Z. Wu, L.P. Huang, B. Zhou, M. Lei, L. Sun, Q. Tian, J. Pan, W. Wu, H. Zhang, Significantly enhanced dye removal performance of hollow tin oxide nanoparticles via carbon coating in dark environment and study of its mechanism, Nanoscale Res. Lett. 9 (2014) 1–9, https://doi.org/10.1186/1556-276X-9-442.
[36] Y.-H. Chin, J.-C. Sin, S.-M. Lam, H. Zeng, H. Lin, H. Li, A.R. Mohamed, 0-D/3-D heterojunction composite constructed by decorating transition metal oxide nanoparticle on peony-like ZnO hierarchical microstructure for improved photodegradation of palm oil mill effluent, Optik (Stuttg). 260 (2022), 169098, https://doi.org/10.1016/j.ijleo.2022.169098.
[37] J.C. Sin, C.A. Lim, S.M. Lam, H. Zeng, H. Lin, H. Li, A.R. Mohamed, Fabrication of novel visible light-driven Nd-doped BiOBr nanosheets with enhanced photocatalytic performance for palm oil mill effluent degradation and Escherichia coli inactivation, J. Phys. Chem. Solids. 140 (2020), 109382, https://doi.org/10.1016/j.jpcs.2020.109382.
[38] S.-M. Lam, J.-C. Sin, H. Zeng, H. Lin, H. Li, Z. Qin, J.W. Lim, A.R. Mohamed, Z-scheme MoO3 anchored-hexagonal rod like ZnO/Zn photoanode for effective wastewater treatment, copper reduction accompanied with electricity production in sunlight-powered photocatalytic fuel cell, Sep. Purif. Technol. 265 (2021) 118495.
[39] J.-M. Jehng, I.E. Wachs, Structural Chemistry and Raman Spectra of Niobium Oxides, Chem. Mater. 3 (1991) 100–107, https://doi.org/10.1021/cm00013a025.
[40] C. Gómez, J. Rodríguez-Páez, The effect of the synthesis conditions on structure and photocatalytic activity of Nb2O5 nanostructures, Process. Appl. Ceram. 12 (3) (2018) 218–229.
[41] A.M. Raba, J. Bautista-Ruiz, M.R. Joya, Synthesis and Structural Properties of Niobium Pentoxide Powders : A Comparative Study of the Growth Process, Mater. Res. 19 (2016) 1381–1387, https://doi.org/10.1590/1980-5373-MR-2015-0733.
[42] M. Palatnikov, O. Shcherbina, N. Sidorov, I. Skab, K. Bormanis, The structure of niobium and tantalum oxides processed by con- centrated light flux, Ukr. J. Phys. Opt. 13 (4) (2012) 207.
[43] F.P. Cardoso, A.E. Nogueira, P.S.O. Patrício, L.C.A. Oliveira, Effect of tungsten doping on catalytic properties of niobium oxide, J. Braz. Chem. Soc. 23 (2012) 702–709, https://doi.org/10.1590/s0103-50532012000400016.
[44] M. Ristić, S. Popović, S. Musić, Sol-gel synthesis and characterization of Nb2O5 powders, Mater. Lett. 58 (2004) 2658–2663, https://doi.org/10.1016/j.matlet.2004.03.041.
[45] D.C. Castro, R.P. Cavalcante, J. Jorge, M.A.U. Martines, L.C.S. Oliveira, G. A. Casagrande, A. Machulek, Synthesis and characterization of mesoporous Nb2O5 and its application for photocatalytic degradation of the herbicide methylviologen, J. Braz. Chem. Soc. 27 (2016) 303–313, https://doi.org/10.5935/0103-5053.20150244.
[46] N. Suzuki, T. Athar, Y.T. Huang, K. Shimasaki, N. Miyamoto, Y. Yamauchi, Synthesis of mesoporous Nb2O5 with crystalline walls and investigation of their photocatalytic activity, J. Ceram. Soc. Japan. 119 (2011) 405–411, https://doi.org/10.2109/jcersj2.119.405.
[47] X. Ma, Y. Chen, H. Li, X. Cui, Y. Lin, Annealing-free synthesis of carbonaceous Nb2O5 microspheres by flame thermal method and enhanced photocatalytic activity for hydrogen evolution, Mater. Res. Bull. 66 (2015) 51–58, https://doi.org/10.1016/j.materresbull.2015.02.005.
[48] Y. Wang, S. Aghamohammadi, D. Li, K. Li, R. Farrauto, Structure dependence of Nb2O5-X supported manganese oxide for catalytic oxidation of propane: Enhanced oxidation activity for MnOx on a low surface area Nb2O5-X, Appl. Catal. B Environ. 244 (2019) 438–447, https://doi.org/10.1016/j.apcatb.2018.11.066.
[49] G.P. Costa, R.A. Rafael, J.C.S. Soares, A.B. Gaspar, Synthesis and characterization of ZnO-Nb2O5catalysts for photodegradation of bromophenol blue, Catal. Today. 344 (2020) 240–246, https://doi.org/10.1016/j.cattod.2019.04.059.
[50] A. Mikolajczyk, A. Gajewicz, B. Rasulev, N. Schaeublin, E. Maurer-gardner, S. Hussain, J. Leszczynski, T. Puzyn, Zeta Potential for Metal Oxide Nanoparticles: A Predictive Model Developed by a Nano-Quantitative Structure − Property Relationship Approach, Chem. Mater. 27 (2015) 2400–2407, https://doi.org/10.1021/cm504406a.
[51] G. Trefalt, B. Malic, D. Kuscer, J. Holc, M. Kosec, Synthesis of Pb(Mg1/3Nb2/3)O3 by Self-Assembled Colloidal Aggregates, J. Am. Ceram. Soc. 94 (2011) 2846–2856, https://doi.org/10.1111/j.1551-2916.2011.04443.x.
[52] L.C.A. Oliveira, M.F. Portilho, A.C. Silva, H.A. Taroco, P.P. Souza, Modified niobia as a bifunctional catalyst for simultaneous dehydration and oxidation of glycerol, Appl. Catal. B, Environ. 117–118 (2012) 29–35, https://doi.org/10.1016/j.apcatb.2011.12.043.
[53] Y.A. Bhembe, L.N. Dlamini, Photoreduction of chromium (VI) by a composite of niobium (V) oxide impregnated with a Ti-based MOF, J. Environ. Sci. Heal. Part A. 55 (8) (2020) 1003–1020.
[54] N. Kumari, K. Gaurav, S.K. Samdarshi, A.S. Bhattacharyya, S. Paul, B. Rajbongshi, K. Mohanty, Solar Energy Materials and Solar Cells Dependence of photoactivity of niobium pentoxide (Nb2O5) on crystalline phase and electrokinetic potential of the hydrocolloid, Sol. Energy Mater. Sol. Cells. 208 (2020), 110408, https://doi.org/10.1016/j.solmat.2020.110408.
[55] F. Azeez, E. Al-hetlani, M. Arafa, Y. Abdelmonem, A.A. Nazeer, M.O. Amin, M. Madkour, The effect of surface charge on photocatalytic degradation of methylene blue dye using chargeable titania nanoparticles, Sci. Rep. 8 (2018) 1–9, https://doi.org/10.1038/s41598-018-25673-5.
[56] T.M. Mok, S.K. O'Leary, The dependence of the Tauc and Cody optical gaps associated with hydrogenated amorphous silicon on the film thickness: αl Experimental limitations and the impact of curvature in the Tauc and Cody plots, J. Appl. Phys. 102 (11) (2007) 113525.
[57] M.E. Sánchez-Vergara, J.C. Alonso-Huitron, A. Rodriguez-Gómez, J.N. Reider-Burstin, Determination of the optical GAP in thin films of amorphous dilithium phthalocyanine using the Tauc and Cody models, Molecules. 17 (2012) 10000–10013, https://doi.org/10.3390/molecules170910000.
[58] J. Tauc, Absorption edge and internal electric fields in amorphous semiconductors, Mater. Res. Bull. 5 (1970) 721–729, https://doi.org/10.1016/0025-5408(70)90112-1.
[59] N.F. Andrade Neto, B.P. Dias, R.L. Tranquilin, E. Longo, M. Li, M.R.D. Bomio, F. V. Motta, Synthesis and characterization of Ag+ and Zn2+ co-doped CaWO4 nanoparticles by a fast and facile sonochemical method, J. Alloys Compd. 823 (2020), 153617, https://doi.org/10.1016/j.jallcom.2019.153617.
[60] W. Choi, A. Termin, M.R. Hoffmann, The Role of Metal Ion Dopants in Quantum-Sized TiO2: Correlation between Photoreactivity and Charge Carrier

Recombination Dynamics, J. Phys. Chem. 98 (1994) 13669–13679, https://doi.org/10.1021/j100102a038.
[61] A. Eshaghi, H. Moradi, Optical and photocatalytic properties of the Fe-doped TiO 2 nanoparticles loaded on the activated carbon, Adv. Powder Technol. 29 (2018) 1879–1885, https://doi.org/10.1016/j.apt.2018.04.026.
[62] P.B. Nair, V.B. Justinvictor, G.P. Daniel, K. Joy, V. Ramakrishnan, D. Devraj, P. V. Thomas, Structural, optical, photoluminescence and photocatalytic investigations on Fe doped Tio 2 thin fi lms, Thin Solid Films. 550 (2014) 121–127, https://doi.org/10.1016/j.tsf.2013.10.112.
[63] S. Sood, A. Umar, S. Kumar, S. Kumar, Highly effective Fe-doped TiO2 nanoparticles photocatalysts for visible- light driven photocatalytic degradation of toxic organic compounds, J. Colloid Interface Sci. 450 (2015) 213–223, https://doi.org/10.1016/j.jcis.2015.03.018.
[64] L. Wang, Y. Li, P. Han, Y. Jiang, Facile fabrication of Fe-doped Nb2O5nanofibers by an electrospinning process and their application in photocatalysis, RSC Adv. 11 (2020) 462–469, https://doi.org/10.1039/d0ra10042k.
[65] P. Nagaraju, R. Vasudevan, A. Alsalme, A. Alghamdi, M. Arivanandhan, R. Jayavel, Surfactant-free synthesis of Nb2O5 nanoparticles anchored graphene nanocomposites with enhanced electrochemical performance for supercapacitor electrodes, Nanomaterials. 10 (1) (2020) 160.
[66] A. Gupta, M. Mittal, M.K. Singh, S.L. Suib, O.P. Pandey, Low temperature synthesis of NbC/C nano-composites as visible light photoactive catalyst, Sci. Rep. 8 (2018) 1–17, https://doi.org/10.1038/s41598-018-31989-z.
[67] F. Zhao, A. Vrajitoarea, Q. Jiang, X. Han, A. Chaudhary, J.O. Welch, R.B. Jackman, Graphene-Nanodiamond Heterostructures and their application to High Current Devices, Sci. Rep. 5 (2015) 17–19, https://doi.org/10.1038/srep13771.
[68] H. Lv, H. Zhao, T. Cao, L. Qian, Y. Wang, G. Zhao, Efficient degradation of high concentration azo-dye wastewater by heterogeneous Fenton process with iron-based metal-organic framework, J. Mol. Catal. A Chem. 400 (2015) 81–89, https://doi.org/10.1016/j.molcata.2015.02.007.
[69] N.K. Gupta, Y. Ghaffari, S. Kim, J. Bae, K.S. Kim, M. Saifuddin, Photocatalytic Degradation of Organic Pollutants over MFe2O4 (M = Co, Ni, Cu, Zn) Nanoparticles at Neutral pH, Sci. Rep. 10 (2020) 1–11, https://doi.org/10.1038/s41598-020-61930-2.
[70] T. Ali, P. Tripathi, A. Azam, W. Raza, A.S. Ahmed, A. Ahmed, M. Muneer, Photocatalytic performance of Fe-doped TiO2 nanoparticles under visible-light irradiation, Mater. Res. Express. 4 (1) (2017) 015022.
[71] H. Moradi, A. Eshaghi, S.R. Hosseini, K. Ghani, Fabrication of Fe-doped TiO2 nanoparticles and investigation of photocatalytic decolorization of reactive red 198 under visible light irradiation, Ultrason. Sonochem. 32 (2016) 314–319, https://doi.org/10.1016/j.ultsonch.2016.03.025.
[72] J. Zhang, D. Li, J. Qiu, Z. Wen, X. Luo, C. Bian, J. Chen, M. Luo, Insights into the photocatalytic degradation of triclosan over amorphous Nb2O5 catalysts, Mater. Res. Expreess. 7 (2020), 115502.
[73] D. Shuang, W. Runwei, Z. Panpan, K. Bonan, Z. Daliang, Z. Zongtao, Q. Shilun, Synthesis and Visible-light Photocatalytic Performance of C-doped Nb2O5 with High Surface Area, Chem. Res. Chinese Univ. 34 (2018) 274–278, https://doi.org/10.1007/s40242-018-7260-9.
[74] C. Zhou, Z. Zeng, G. Zeng, D. Huang, R. Xiao, M. Cheng, C. Zhang, W. Xiong, C. Lai, Y. Yang, W. Wang, H. Yi, B. Li, Visible-light-driven photocatalytic degradation of sulfamethazine by surface engineering of carbon nitride:Properties, degradation pathway and mechanisms, J. Hazard. Mater. 380 (2019), 120815, https://doi.org/10.1016/j.jhazmat.2019.120815.
[75] N.F. Andrade Neto, L.E. Nascimento, M. Correa, F. Bohn, M.R.D. Bomio, F. V. Motta, Characterization and photocatalytic application of Ce4+, Co2+, Mn2+ and Ni2+ doped Fe3O4 magnetic nanoparticles obtained by the co-precipitation method, Mater. Chem. Phys. 242 (2020) 122489.
[76] M.R. Delsouz Khaki, M.S. Shafeeyan, A.A.A. Raman, W.M.A.W. Daud, Evaluating the efficiency of nano-sized Cu doped TiO2/ZnO photocatalyst under visible light irradiation, J. Mol. Liq. 258 (2018) 354–365, https://doi.org/10.1016/j.molliq.2017.11.030.
[77] S. Qourzal, I. Bakas, N. Barka, A. Assabbane, Y. Ait-ichou, Factorial Experimental Design for the Optimization of β-Naphthol Photocatalytic Degradation in TiO2 Aqueous Suspension, Can. Chem. Trans. 2 (2014) 1–11, https://doi.org/10.13179/canchemtrans.2014.02.01.0046.
[78] E.T. De Jesus, A.J. Moreira, M.C. Sá, G. Paulo, G. Freschi, M.R. Joya, M.S. Li, E. C. Paris, E.C. Paris, Potential of Nb 2 O 5 nanofibers in photocatalytic degradation of organic pollutants, Environ. Sci. Pollut. Res. 28 (2021) 69401–69415.
[79] G. Sharifzade, A. Asghari, M. Rajabi, Highly effective adsorption of xanthene dyes (rhodamine B and erythrosine B) from aqueous solutions onto lemon citrus peel active carbon: Characterization, resolving analysis, optimization and mechanistic studies, RSC Adv. 7 (2017) 5362–5371, https://doi.org/10.1039/c6ra23157h.